

## Article

# CaH<sub>2</sub>-Assisted Molten Salt Synthesis of Zinc-Rich Intermetallic Compounds of RhZn<sub>13</sub> and Pt<sub>3</sub>Zn<sub>10</sub> for Catalytic Selective Hydrogenation Application

Yasukazu Kobayashi <sup>1,\*</sup>, Koharu Yamamoto <sup>2</sup> and Ryo Shoji <sup>2</sup>

<sup>1</sup> Renewable Energy Research Centre, National Institute of Advanced Industrial Science and Technology, 2-2-9 Machiikedai, Koriyama 963-0298, Japan

<sup>2</sup> Department of Chemical Science and Engineering, National Institute of Technology, Tokyo College, 1220-2 Kunugida, Hachioji 193-0997, Japan; yamamotokoharu.09@gmail.com (K.Y.); shoji@tokyo-ct.ac.jp (R.S.)

\* Correspondence: yasu-kobayashi@aist.go.jp

**Abstract:** Zinc-included intermetallic compound catalysts of RhZn, PtZn, and PdZn with a molar ratio of Zn/metal = 1/1, which are generally prepared using a hydrogen reduction approach, are known to show excellent catalytic performance in some selective hydrogenations of organic compounds. In this study, in order to reduce the incorporated amounts of the expensive noble metals, we attempted to prepare zinc-rich intermetallic compounds via a CaH<sub>2</sub>-assisted molten salt synthesis method with a stronger reduction capacity than the common hydrogen reduction method. X-ray diffraction results indicated the formation of RhZn<sub>13</sub> and Pt<sub>3</sub>Zn<sub>10</sub> in the samples prepared by the reduction of ZnO-supported metal precursors. In a hydrogenation reaction of *p*-nitrophenol to *p*-aminophenol, the ZnO-supported RhZn<sub>13</sub> and Pt<sub>3</sub>Zn<sub>10</sub> catalysts showed a higher selectivity than the RhZn/ZnO and PtZn/ZnO catalysts with the almost similar conversions. Thus, it was demonstrated that the zinc-rich intermetallic compounds of RhZn<sub>13</sub> and Pt<sub>3</sub>Zn<sub>10</sub> could be superior selective hydrogenation catalysts compared to the conventional intermetallic compound catalysts of RhZn and PtZn.

**Keywords:** molten salt synthesis; CaH<sub>2</sub>; intermetallic compound; RhZn<sub>13</sub>; Pt<sub>3</sub>Zn<sub>10</sub>; hydrogenation of *p*-nitrophenol; selective hydrogenation; water remediation



**Citation:** Kobayashi, Y.; Yamamoto, K.; Shoji, R. CaH<sub>2</sub>-Assisted Molten Salt Synthesis of Zinc-Rich Intermetallic Compounds of RhZn<sub>13</sub> and Pt<sub>3</sub>Zn<sub>10</sub> for Catalytic Selective Hydrogenation Application. *Crystals* **2024**, *14*, 278. <https://doi.org/10.3390/cryst14030278>

Academic Editor: Andrei Vladimirovich Shevelkov

Received: 28 February 2024

Revised: 11 March 2024

Accepted: 11 March 2024

Published: 15 March 2024



**Copyright:** © 2024 by the authors. Licensee MDPI, Basel, Switzerland. This article is an open access article distributed under the terms and conditions of the Creative Commons Attribution (CC BY) license (<https://creativecommons.org/licenses/by/4.0/>).

## 1. Introduction

Hydrogenation is one of the important processes used to refine intermediate compounds in the petrochemical industry and has mainly depended on precious metal-based catalysts for a long time [1]. Although noble metals, such as Pd, Pt, and Rh, are attractive hydrogenation catalysts due to their excellent catalytic performance, they are expensive and rare. Therefore, alloying catalysts have been studied intensively to decrease the amounts of metals required while improving the catalytic activity via changes in electronic properties and configurations of surface-exposed elements [2–4]. Recently, zinc-incorporated alloys have been developed as fascinating hydrogenation catalysts because of the lower cost of zinc and availability of the component metals [5–8]. As summarized in Table 1, zinc alloy catalysts with Rh, Pt, and Pd in molar ratios of Zn/M ≤ 1 (M = Rh, Pt, or Pd) have been proved to work as excellent hydrogenation catalysts with improved selectivity and/or activity in several industrially important hydrogenation reactions of organic compounds. The nanoscale zinc alloy catalysts are commonly prepared by partially reducing ZnO support to form the alloyed nanoparticles with loaded metals under a H<sub>2</sub> gas flow at high temperatures of ≥400 °C. Since ZnO is a stable oxide, and intermetallic phases with a molar ratio of Zn/M = 1/1 are also stable crystal structures, it is difficult to prepare zinc-rich alloy catalysts throughout the H<sub>2</sub> reduction treatment. In our searches of the literature, most of the reported zinc alloy catalysts are those in molar ratios of Zn/M ≤ 1, especially RhZn,

PtZn, and PdZn, and, thus, zinc-rich alloy catalysts are not yet reported for the catalyst application.

In this study, we attempted to develop zinc-rich intermetallic catalysts with Rh, Pt, and Pd via a CaH<sub>2</sub>-assisted molten salt synthesis method with a stronger reduction capacity than the common hydrogen reduction method. Molten salt synthesis is a good technique to obtain active catalysts [9–12]. Previously, we prepared some nanosized intermetallic compounds using the CaH<sub>2</sub>-assisted molten salt synthesis [13] and exhibited that some are available as good catalyst supports, such as Ti<sub>6</sub>Si<sub>7</sub>Ni<sub>16</sub> [14], and some are active species, such as TiNi [15], YIr<sub>2</sub> [16], CaPt<sub>2</sub> [17]. In a reduction condition with a CaH<sub>2</sub> reducing agent in a molten LiCl-KCl at 360 °C, ZnO was totally reduced to metallic zinc to alloy with metallic Ni, following a formation of intermetallic compound NiZn [18]. Because ZnO was not reduced for the alloying with Ni in a common reduction condition of H<sub>2</sub> gas flow at 360 °C, it was demonstrated that the CaH<sub>2</sub>-assisted molten salt approach had a higher reduction capacity than the common hydrogen gas reduction. Thus, the molten salt method has a high potential to prepare zinc-rich intermetallic compounds at a low reduction temperature, enabling the formation of nanosized alloys. Finally, the prepared alloy catalysts were tested in hydrogenation of *p*-nitrophenol (4-NP) to *p*-aminophenol (4-AP) with NaBH<sub>4</sub> as a model hydrogenation reaction so as to evaluate catalytic activities and/or selectivities of the prepared zinc-rich intermetallic compounds.

**Table 1.** Previous reports of hydrogenation of organic compounds catalyzed by zinc alloys of RhZn, PtZn, and PdZn.

Active Alloys	Hydrogenation Reactions	Ref.
RhZn	Selective hydrogenation of nitroarene	[19]
	Selective hydrogenation of dienes to monoenes	[20]
PtZn	Selective hydrogenation of crotonaldehyde	[21–23]
	Selective hydrogenation of 4-nitrophenylacetylene	[24,25]
	Selective hydrogenation of halonitrobenzene to haloaniline	[26]
	Hydrogenation of diphenylacetylene	[27]
PdZn	Semi-hydrogenation of Alkyne	[28–30]
	Semi-hydrogenation of acetylene	[31–43]
	Semi-hydrogenation of alkynols	[44–47]
	Hydrogenation of 1-Butene and 1,3-Butadiene Mixtures	[48,49]
	Hydrogenation of 2-methyl-3-butyn-2-ol	[50–52]
	Selective hydrogenation of nitrostyrene to aminostyrene	[53]
Hydrogenation of cinnamaldehyde to hydrocinnamyl alcohol	[54]	
Selective hydrogenative rearrangement of furan compounds	[55]	

## 2. Materials and Methods

First, ZnO-supported metal precursors were prepared by a common impregnation method. RhCl<sub>3</sub>·3H<sub>2</sub>O (99.5%, Wako Pure Chem. Corp., Osaka, Japan), H<sub>2</sub>PtCl<sub>6</sub>·6H<sub>2</sub>O (98.5%, Wako Pure Chem. Corp., Osaka, Japan), and (NH<sub>4</sub>)<sub>2</sub>PdCl<sub>4</sub> (97%, Sigma-Aldrich Japan K.K., Tokyo, Japan) were separately dissolved in distilled water, and then ZnO nanopowder (10–25 m<sup>2</sup>/g, <100 nm particle size, Sigma-Aldrich Japan K.K., Tokyo, Japan) was put into each solution with a weight ratio of M(=Rh, Pt or Pd)/ZnO = 5/95. The suspensions were then dried at 120 °C and calcinated at 500 °C for 2 h. The obtained powders were named as Rh/ZnO(Pre), Pt/ZnO(Pre), and Pd/ZnO(Pre), respectively. Next, reduced catalysts were obtained by reducing the above precursors in two different reduction conditions: (1) hydrogen reduction and (2) CaH<sub>2</sub> reduction in molten LiCl-KCl. For the (1) hydrogen reduction, each precursor was reduced in a hydrogen gas flow of 50 mL/min at 380 °C for 5 h. The obtained powders were denoted as Rh/ZnO(H), Pt/ZnO(H), and Pd/ZnO(H), respectively. For the (2) CaH<sub>2</sub> reduction in molten LiCl-KCl, each precursor, CaH<sub>2</sub> (JUNSEI Chem. Co., Ltd., Tokyo, Japan), LiCl (Wako Pure Chem. Corp., Osaka, Japan), and KCl (Wako Pure Chem. Corp., Osaka, Japan) was mixed in a mortar in a weight

ratio of precursor/LiCl/KCl/CaH<sub>2</sub> = 0.3/0.14/0.16/0.6. The mixed powder was then loaded in a stainless-steel reactor connected with an argon gas flow of 50 mL/min and heated at 380 °C for 5 h. After the cool down to room temperature, the treated samples were crushed in a mortar. The obtained powders were rinsed with 0.1 M NH<sub>4</sub>Cl aqueous solution to remove any calcium-related impurities, especially CaO dissolved in the solution, and finally with distilled water to remove water-soluble compounds. The obtained powders were denoted as Rh/ZnO(CLK), Pt/ZnO(CLK), and Pd/ZnO(CLK), respectively.

The crystal structure of the obtained samples was examined by X-ray diffraction (XRD, SmartLab, 3 kW, Rigaku, Tokyo, Japan) with CuK<sub>α</sub> radiation at 40 kV and 30 mA. The measurements ranged from 20° to 70° with a step interval of 0.01° and a scan speed of 10°/min. The porosity was investigated by N<sub>2</sub> adsorption and desorption at -196 °C (BELLSORP mini-II, MicrotracBEL Corp., Osaka, Japan). The sample was pre-treated at 150 °C for 1 h under vacuum before the measurement. The morphology with energy dispersive X-ray spectrometry (EDX) for elemental analysis was observed by a scanning electron microscope (SEM, JSM-7800 F, JEOL, Ltd., Tokyo, Japan). The chemical states and composition of the prepared samples' surface were determined using X-ray photoelectron spectroscopy (XPS) (PHI X-tool, ULVAC-PHI, Inc., Kanagawa, Japan) operated with AlK<sub>α</sub> radiation. The chemical shifts were calibrated by fixing the C 1s peak of the surface carbonaceous contaminants at 284.5 eV. The identification of the obtained signals was conducted by using the reference book.

The catalytic hydrogenation of 4-NP to 4-AP was conducted with the prepared samples and ZnO for reference. The catalytic reactions were conducted in 20 mL glass bottles following the previously reported procedures. In the catalytic tests, 1 mL of 4-NP solution (14 mM) was added to a bottle containing 10 mg of catalyst powder, 1 mL of NaBH<sub>4</sub> solution (0.42 M), and 7 mL of distilled water as the solvent. To satisfy first-order reaction kinetics, the initial concentration of NaBH<sub>4</sub> (0.047 M) was 30 times higher than that of 4-NP (1.6 mM). The reactions were stirred at 25 °C for 60 min. An aluminum heat sink mounted on a hotplate was used to maintain a constant solution temperature. A small aliquot (100 μL) solution was taken to determine the concentration changes at reaction times of 0.5–60 min. The conversion and selectivity of 4-NP to 4-AP were monitored using an ultraviolet-visible spectrometer using the respective absorbance changes at 401 and 313 nm.

### 3. Results and Discussion

#### 3.1. Preparation of Zinc-Rich Intermetallic Compounds

X-ray diffraction measurements were conducted to identify the crystal structures in the prepared samples. Identified compounds are summarized in Table 2. For the Rh-Zn samples of Rh/ZnO(Pre), Rh/ZnO(CLK), and Rh/ZnO(H), the observed XRD patterns are shown in Figure 1. The main crystal structure was ZnO for all the samples with a main peak observed at 36°, which was a reasonable result because ZnO was intended to occupy 95 wt% of the samples. In addition, some unknown peaks were observed for Rh/ZnO(Pre). These peaks were also observed for the other precursors of Pt/ZnO(Pre) and Pd/ZnO(Pre), so the peaks could be assigned to any compounds included in the used ZnO. As for the Rh species, the identified species was Rh<sub>2</sub>O<sub>3</sub> for Rh/ZnO(Pre). The peaks identified for Rh<sub>2</sub>O<sub>3</sub> and metallic Rh were not observed in the reduced samples of Rh/ZnO(CLK) and Rh/ZnO(H), suggesting the formation of alloyed species with Zn. A peak at 29.4 ° could be assigned to a main peak of a (104) facet of CaCO<sub>3</sub> for Rh/ZnO(CLK). As shown in Figure 1b, a resolution of the observed peaks for Rh/ZnO(CLK) was low, but they are nicely identified for the reference peaks of RhZn<sub>13</sub>. A peak assigned to a main peak of reference RhZn at 42.6° was observed for Rh/ZnO(H). Thus, it was confirmed that Rh<sub>2</sub>O<sub>3</sub> was reduced by the reduction treatments of (1) hydrogen reduction and (2) CaH<sub>2</sub> reduction in molten LiCl-KCl to form RhZn and RhZn<sub>13</sub>, respectively, by alloying with the reduced Rh and Zn of some part of ZnO.

**Table 2.** Summary of experimental results by nitrogen adsorptions, XRD measurements, and XPS measurements for ZnO and the prepared samples.

Sample	Active Metal	BET S. A. [m <sup>2</sup> /g]	XRD Measurements		XPS Measurements	
			Zn Species	Metal Species	Main Chemical States of Metals	Molar Ratios of Metal/Zn [mol/mol]
ZnO	None	12.7	ZnO	None	None	None
Rh/ZnO(Pre)	Rh	12.5	ZnO	Rh <sub>2</sub> O <sub>3</sub>	Rh(+3)	0.101
Rh/ZnO(CLK)		20.4	ZnO	RhZn <sub>13</sub>	Rh(0)	0.046
Rh/ZnO(H)		4.8	ZnO	RhZn	Rh(0)	0.028
Pt/ZnO(Pre)	Pt	7.4	ZnO	Unknown	Oxides	0.049
Pt/ZnO(CLK)		19.2	ZnO	Pt <sub>3</sub> Zn <sub>10</sub>	Pt(0)	0.128
Pt/ZnO(H)		6.5	ZnO	PtZn	Pt(0)	0.017
Pd/ZnO(Pre)	Pd	5.2	ZnO	Pd	Pd(+2, +4)	0.058
Pd/ZnO(CLK)		17.1	ZnO	Distorted Pd <sub>5</sub> Zn <sub>8</sub>	Pd(0)	0.011
Pd/ZnO(H)		4.5	ZnO	PdZn	Pd(0)	0.060

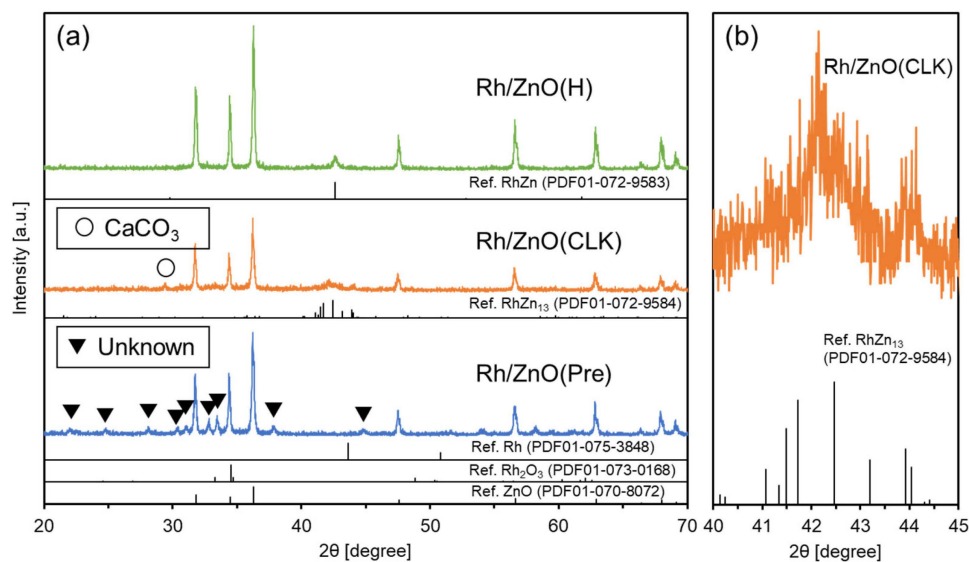
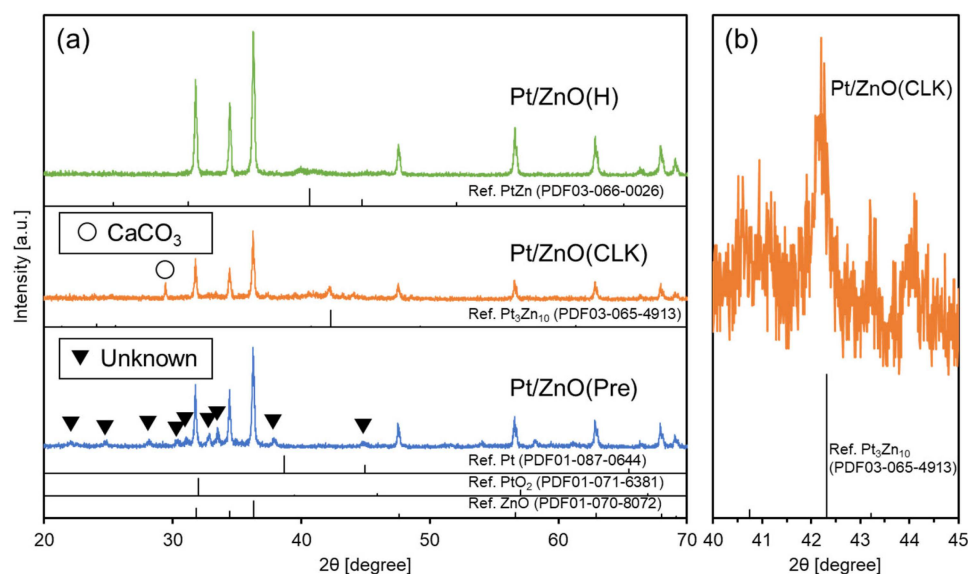
**Figure 1.** XRD patterns of Rh/ZnO(H), Rh/ZnO(CLK), and Rh/ZnO(Pre) in (a) a wide range scale and (b) a narrow range scale for Rh/ZnO(CLK).

Figure 2 shows the XRD patterns of Pt/ZnO(Pre), Pt/ZnO(CLK), and Pt/ZnO(H). The main peaks observed around 30–40° were identified for ZnO for all the samples. In addition, some unknown peaks were also observed for Pt/ZnO(Pre), which was similar to Rh/ZnO(Pre) and Pd/ZnO(Pre). So, the peaks could be assigned to any compounds included in the used ZnO. As for the Pt species, the observed peaks were not identified for PtO<sub>2</sub> and metallic Pt in Pt/ZnO(Pre), suggesting the formation of amorphous oxide species and/or species that were too small to be detected by XRD. The peaks identified for PtO<sub>2</sub> and metallic Pt were not observed in the reduced samples of Pt/ZnO(CLK) and Pt/ZnO(H), suggesting the formation of alloyed species with Zn. A peak at 29.4° could be assigned to a main peak of a (104) facet of CaCO<sub>3</sub> for Pt/ZnO(CLK). As shown in Figure 2b, a resolution of the observed peaks for Pt/ZnO(CLK) was low, but a peak is nicely identified to the main reference peak of Pt<sub>3</sub>Zn<sub>10</sub>. A peak assigned to a main peak of reference PtZn at 40.6° was observed for Pt/ZnO(H). Thus, the results confirmed the formation of zinc alloys of PtZn and Pt<sub>3</sub>Zn<sub>10</sub> in Pt/ZnO(H) and Pt/ZnO(CLK), respectively, by the different reduction treatments of (1) hydrogen reduction and (2) CaH<sub>2</sub> reduction in molten LiCl-KCl.



**Figure 2.** XRD patterns of Pt/ZnO(H), Pt/ZnO(CLK), and Pt/ZnO(Pre) in (a) a wide range scale and (b) a narrow range scale for Pt/ZnO(CLK).

Figure 3 shows the XRD patterns of Pd/ZnO(Pre), Pd/ZnO(CLK), and Pd/ZnO(H). Similar to the samples mentioned above, the main peaks observed around 30–40° were identified as ZnO for all the samples. In addition, some unknown peaks were also observed for Pd/ZnO(Pre), which was similar to Rh/ZnO(Pre) and Pt/ZnO(Pre). Thus, the peaks could be assigned to any compounds included in the used ZnO. As for the Pd species, the identified species was metallic Pd for Pd/ZnO(Pre). The peaks identified for PdO and metallic Pd were not observed in the reduced samples of Pd/ZnO(CLK) and Pd/ZnO(H), suggesting the formation of alloyed species with Zn in a similar manner to the above Rh-/Pt-based samples. In addition to the peaks assigned to ZnO, a large peak was observed at 42.2° for Pd/ZnO(CLK). According to the database, any reference compounds with Pd and/or Zn were not identified for the observed peak. A main peak of reference, Pd<sub>5</sub>Zn<sub>8</sub>, is located at 41.9°, which is close to the position of the observed peak. Therefore, it was concluded that the distorted Pd<sub>5</sub>Zn<sub>8</sub> could be formed in Pd/ZnO(CLK). The peaks assigned to reference PdZn were perfectly observed for Pt/ZnO(H). In sum, the XRD results suggested the formation of zinc alloys of PdZn and distorted Pd<sub>5</sub>Zn<sub>8</sub> in Pd/ZnO(H) and Pd/ZnO(CLK), respectively, by the different reduction treatments of (1) hydrogen reduction and (2) CaH<sub>2</sub> reduction in molten LiCl-KCl.

To confirm the porosities, nitrogen adsorption experiments were conducted for all the prepared samples. The obtained BET surface areas are summarized in Table 2. The BET surface areas of Rh/ZnO(CLK), Pt/ZnO(CLK), and Pd/ZnO(CLK) were larger than those of the other samples. These results indicated that the BET surface areas of Rh/ZnO(Pre), Pt/ZnO(Pre), and Pd/ZnO(Pre) were increased by the following treatment of CaH<sub>2</sub> reduction in molten LiCl-KCl. The CaH<sub>2</sub> reduction treatment may change precursors' morphologies more finely. Next, to confirm the morphologies, SEM observations were performed for the samples treated with a CaH<sub>2</sub> reduction in molten LiCl-KCl. Elemental analyses were also performed by EDX. Figures 4–6 show the results of SEM-EDX for Rh/ZnO(CLK), Pt/ZnO(CLK), and Pd/ZnO(CLK), respectively. In Figure 4, a large bulky particle in a micron meter range can be seen, but fine morphology is also visible on the surface for Rh/ZnO(CLK). Since the measured BET surface area of 20.4 m<sup>2</sup>/g of Rh/ZnO(CLK) was larger than 12.5 m<sup>2</sup>/g and 4.8 m<sup>2</sup>/g of Rh/ZnO(Pre) and Rh/ZnO(H), respectively, it was suggested that Rh/ZnO(CLK) had a finer morphology due to the surface modification via CaH<sub>2</sub> reduction treatment, resulting in an increase in the surface area. In addition, ZnO commercial nanoparticles of <100 nm with 10–25 m<sup>2</sup>/g were used. Thus, the observed particle in a micron meter range could be formed by the aggregation of ZnO nanoparticles.

According to the elemental analysis by EDX, the detected elements were Rh, Zn, O, and Ca with a molar ratio of Rh/Zn/O/Ca = 1.4/79.2/17.3/2.1. As expected, the main elements were Zn and O, originating from ZnO, and the existence of Rh was surely confirmed in the Rh/ZnO(CLK). A negligible amount of Ca was also detected. As a final step in the preparation procedure, the sample was rinsed with  $\text{NH}_4\text{Cl}$  solution to remove CaO and then with distilled water to remove soluble salts, such as  $\text{CaCl}_2$  and LiCl. This was done so that the detected impurities of Ca could be totally removed from the final sample using more rigorous rinsing treatments. As the results of elemental mappings of Rh, Zn, and O show, a good distribution of the elements was clearly observed in the particle, suggesting the homogeneous distribution of the Rh-Zn alloy.

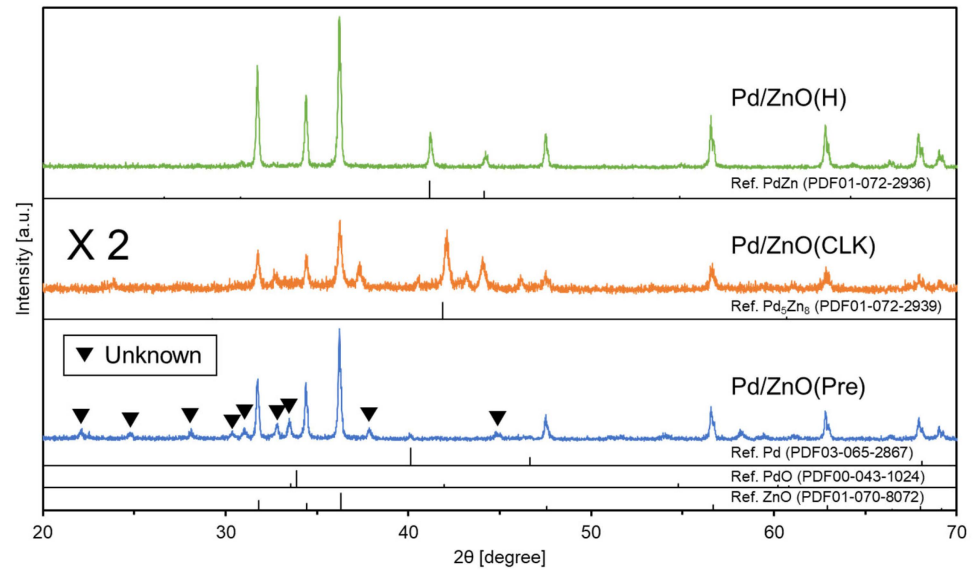


**Figure 3.** XRD patterns of Pd/ZnO(H), Pd/ZnO(CLK), and Pd/ZnO(Pre) in a wide range scale.

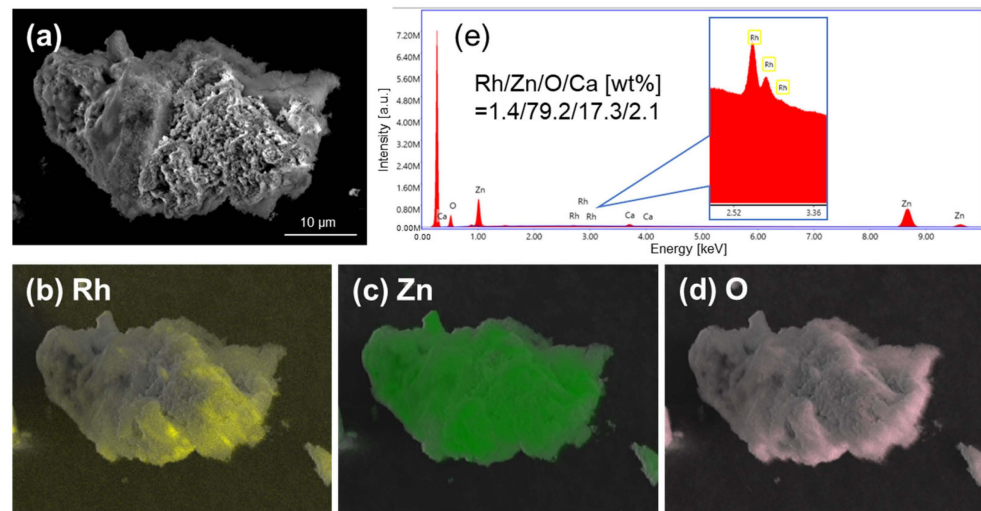


**Figure 4.** (a) SEM image and the corresponding elemental mappings of (b) Rh, (c) Zn, and (d) O for Rh/ZnO(CLK) with (e) an EDX spectrum giving a weight percentage of Rh/Zn/O/Ca = 1.4/79.2/17.3/2.1.

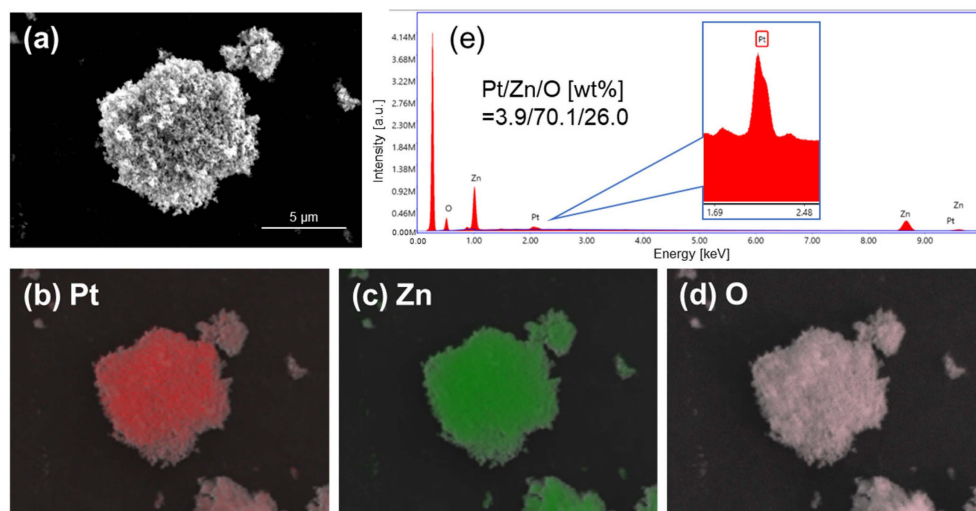


**Figure 5.** (a) SEM image and the corresponding elemental mappings of (b) Pt, (c) Zn, and (d) O for Pt/ZnO(CLK) with (e) an EDX spectrum giving a weight percentage of Pt/Zn/O = 3.9/70.1/26.0.

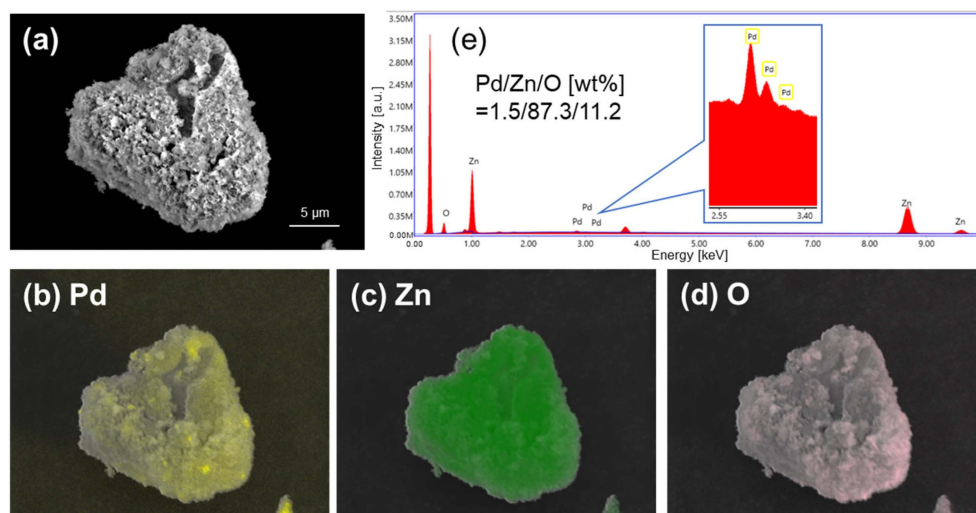


**Figure 6.** (a) SEM image and the corresponding elemental mappings of (b) Pd, (c) Zn, and (d) O for Pd/ZnO(CLK) with (e) an EDX spectrum giving a weight percentage of Pd/Zn/O = 1.5/87.3/11.2.

In Figure 5, a large bulky particle in a micron meter range can be seen, but fine morphology is also visible on the surface for Pt/ZnO(CLK). Since the measured BET surface area of 19.2 m<sup>2</sup>/g of Pt/ZnO(CLK) was larger than 7.4 m<sup>2</sup>/g and 6.5 m<sup>2</sup>/g of Pt/ZnO(Pre) and Pt/ZnO(H), respectively, it was suggested that Pt/ZnO(CLK) had a finer morphology due to the surface modification via CaH<sub>2</sub> reduction treatment, resulting in an increase in the surface area. According to the elemental analysis by EDX, the detected elements were Pt, Zn, and O, with a molar ratio of Pt/Zn/O = 3.9/70.1/26.1. As expected, the main elements were Zn and O, originating from ZnO, and the existence of Pt was surely confirmed in the Pt/ZnO(CLK). As the results of elemental mappings of Pt, Zn, and O show, a good distribution of the elements was clearly observed in the particle, suggesting the homogeneous distribution of Pt-Zn alloy.

In Figure 6, a large bulky particle in a micron meter range can be seen, but fine morphology is also visible on the surface for Pd/ZnO(CLK). Since the measured BET surface area of 17.1 m<sup>2</sup>/g of Pd/ZnO(CLK) was larger than 5.2 m<sup>2</sup>/g and 4.5 m<sup>2</sup>/g of Pd/ZnO(Pre) and Pd/ZnO(H), respectively, it was suggested that Pd/ZnO(CLK) had a finer morphology due to the surface modification via CaH<sub>2</sub> reduction treatment, resulting in the increase in the surface area. According to the elemental analysis by EDX, the detected

elements were Pd, Zn, and O, with a molar ratio of Pd/Zn/O = 1.5/87.3/11.2. As expected, the main elements were Zn and O, originating from ZnO, and the existence of Pd was surely confirmed in the Pd/ZnO(CLK). As the results of elemental mappings of Pd, Zn, and O, a good distribution of the elements was clearly observed in the particle, suggesting the homogeneous distribution of Pd-Zn alloy.

### 3.2. Catalytic Tests with the Prepared Samples

Heterogeneous catalysis reaction occurs on a solid catalyst surface. Therefore, it is important to analyze the surface species before discussing the active species catalyzing the reaction. Figure 7 shows the results of XPS measurements for the prepared samples. Figure 7a shows the XPS spectra of the C 1s of all the samples in which signal tops were moved to 284.5 eV for the calibration of data. Figure 7b shows the XPS spectra of Rh 3d<sub>5/2</sub>, Pt 4d<sub>7/2</sub>, and Pd 3d<sub>5/2</sub> for Rh/ZnO, Pt/ZnO, and Pd/ZnO, respectively. The obtained chemical states of metals and the molar ratios of metal/Zn were summarized in Table 2. In the Rh/ZnO, a peak assigned to Rh<sub>2</sub>O<sub>3</sub> was observed around 308–309 eV for Rh/ZnO(Pre), whereas small peaks assigned to zero-valent Rh were observed at a lower binding energy of 307 eV for Rh/ZnO(CLK) and Rh/ZnO(H). These results supported the XRD results, indicating the formation of Rh oxide in Rh/ZnO(Pre) and Rh alloy in Rh/ZnO(CLK) and Rh/ZnO(H). In Pt/ZnO, a peak assigned to Pt oxides was observed around 74–75 eV for Pt/ZnO(Pre), whereas peaks assigned to zero-valent Pt were observed at a lower binding energy of 71 eV for Pt/ZnO(CLK) and Pt/ZnO(H). These results supported the XRD results, indicating the formation of Pt alloy in Pt/ZnO(CLK) and Pt/ZnO(H). In the Pd/ZnO, a peak was observed between the binding energies assigned to PdO at 336 eV and PdO<sub>2</sub> at 338 eV for Pd/ZnO(Pre), indicating that Pd existed as oxides with a valence of +2~+4. On the other hand, small peaks assigned to zero-valent Pd were observed at a lower binding energy of 335–336 eV for Pd/ZnO(CLK) and Pd/ZnO(H). These results supported the XRD results, indicating the formation of Pd alloy in Pd/ZnO(CLK) and Pd/ZnO(H).

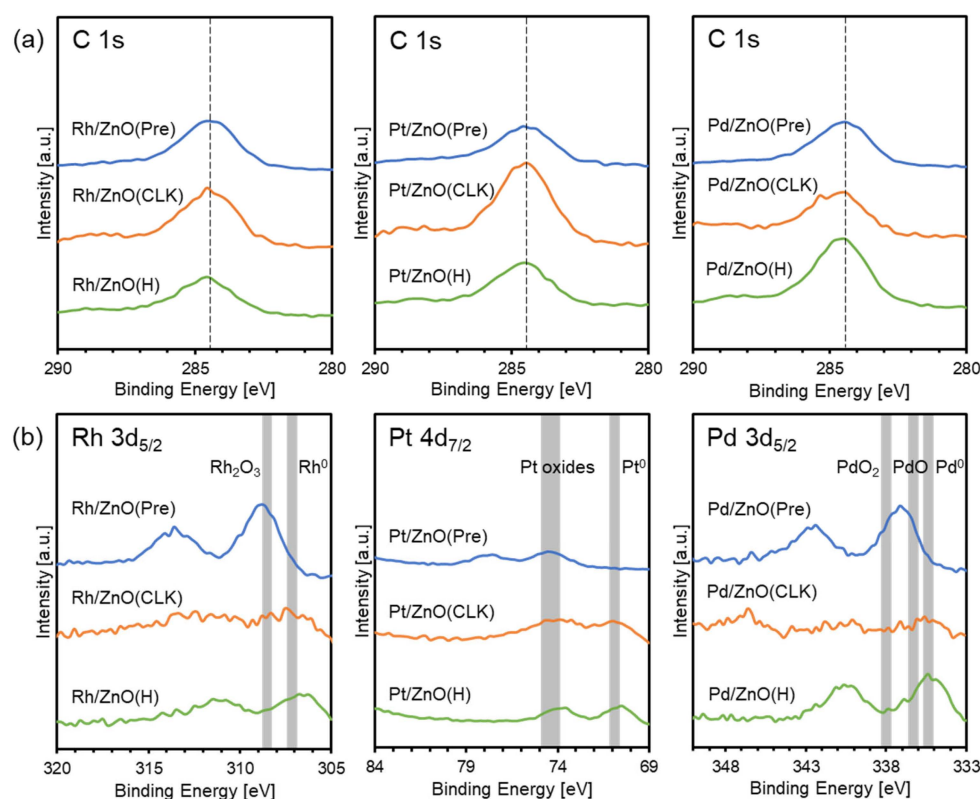


**Figure 7.** XPS spectra of (a) C 1s, and (b) Rh 3d<sub>5/2</sub>, Pt 4d<sub>7/2</sub>, and Pd 3d<sub>5/2</sub> for Rh/ZnO, Pt/ZnO, and Pd/ZnO, respectively.

Catalytic tests were carried out to evaluate the catalytic performance of the prepared samples in hydrogenation of 4-NP to 4-AP with  $\text{NaBH}_4$  as a model hydrogenation reaction. On the left side of Figure 8a–c, normalized concentration ( $C/C_0$ ) changes of 4-NP as functions of reaction times are shown for Rh/ZnO, Pt/ZnO, and Pd/ZnO, respectively, whereas, on the right side of Figure 8a–c, are plots of  $\ln(C/C_0)$  as functions of reaction times for Rh/ZnO, Pt/ZnO, and Pd/ZnO. In Figure 8a, the result with a commercial ZnO was also displayed for reference. The result verified that the concentration did not change with only the ZnO, not including any other metals, such as Rh, Pt, and Pd. For the Rh/ZnO (Figure 8a), the concentration gradually decreased with the reaction time, but the faster reaction rates were given as an order of Rh/ZnO(H) > Rh/ZnO(CLK) > Rh/ZnO(Pre). In the plot of  $\ln(C/C_0)$  as functions of reaction times, good linearities were obtained for all the samples, indicating that the first-order reaction kinetics were satisfied well in the experiments, and the obtained rate constants from the gradients were summarized in Table 3. For the Pt/ZnO (Figure 8b), the concentration gradually decreased with the reaction time, but the faster reaction rates were given as an order of Pt/ZnO(CLK) > Pt/ZnO(H) > Pt/ZnO(Pre). In the plot of  $\ln(C/C_0)$ , as functions of reaction times, good linearities were obtained for all the samples, indicating that the first-order reaction kinetics were satisfied well in the experiments and the obtained rate constants from the gradients were summarized in Table 3. For the Pd/ZnO (Figure 8c), the concentrations quickly decreased to reach zero after 10 min for Pd/ZnO(Pre) and Pd/ZnO(H), whereas the concentration slowly decreased to reach zero after 60 min for Pd/ZnO(CLK). Thus, the faster reaction rates were given as an order of Pd/ZnO(Pre), Pd/ZnO(H)  $\gg$  Pd/ZnO(CLK). Since the peak of Pd  $3d_{5/2}$  in the XPS measurement was too small (Figure 7b) and a very small molar ratio of Pd/Zn (0.011 [mol/mol] as shown in Table 2) was obtained for Pd/ZnO(CLK), it was assumed that Pd/ZnO(CLK) had a much lesser amount of Pd than Pd/ZnO(Pre) and Pd/ZnO(H) on the surface. Probably, most of the Pd could be covered by ZnO and only a very small amount of Pd exposed to the surface catalyzed the reaction in the Pd/ZnO(CLK). In the plot of  $\ln(C/C_0)$  as functions of reaction times, good linearities were obtained for all the samples, indicating that the first-order reaction kinetics were satisfied well in the experiments, and the obtained rate constants from the gradients were summarized in Table 3. Reaction rate constants ( $k$ ) of previous studies with Rh, Pt, and Pd catalysts are also summarized in Table 3. Because the reaction conditions differed, a quantitative comparison was difficult. In the previous studies, Pd catalysts show higher rate constants than Rh and Pt catalysts, and Rh and Pt catalysts give nearly the same constants as each other. The trend is in good agreement with the results of this study.

The obtained conversions and selectivities of 4-NP to 4-AP after 60 min are summarized in Figure 9. In comparison with Rh/ZnO(CLK) and Rh/ZnO(H), the conversions were almost the same as each other after 60 min. However, the selectivity with Rh/ZnO(CLK) was 89%, which was slightly higher than the 82% with Rh/ZnO(H). In comparison with Pt/ZnO(CLK) and Pt/ZnO(H), Pt/ZnO(CLK) exhibited higher conversion and selectivity than Pt/ZnO(H) after 60 min. In comparison with Pd/ZnO(CLK) and Pd/ZnO(H), the conversions and selectivities were almost the same as each other after 60 min.

Interestingly, it was demonstrated that Rh/ZnO(CLK) and Pt/ZnO(CLK) exhibited higher selectivities than Rh/ZnO(H) and Pt/ZnO(H), respectively. According to the results of XRD and XPS discussed above, Rh/ZnO(CLK) and Pt/ZnO(CLK) had  $\text{RhZn}_{13}$  and  $\text{Pt}_3\text{Zn}_{10}$  as active metal species, whereas Rh/ZnO(H) and Pt/ZnO(H) had RhZn and PtZn. These comparisons can lead us to the conclusion that the zinc-rich intermetallic compounds of  $\text{RhZn}_{13}$  and  $\text{Pt}_3\text{Zn}_{10}$  could be superior selective hydrogenation catalysts than the conventional intermetallic compound catalysts of RhZn and PtZn, respectively. Since  $\text{RhZn}_{13}$  and  $\text{Pt}_3\text{Zn}_{10}$  contain smaller amounts of Rh and Pt than RhZn and PtZn,  $\text{RhZn}_{13}$  and  $\text{Pt}_3\text{Zn}_{10}$  can be inexpensive selective hydrogenation catalysts, leading to promising catalysts for industrial application.

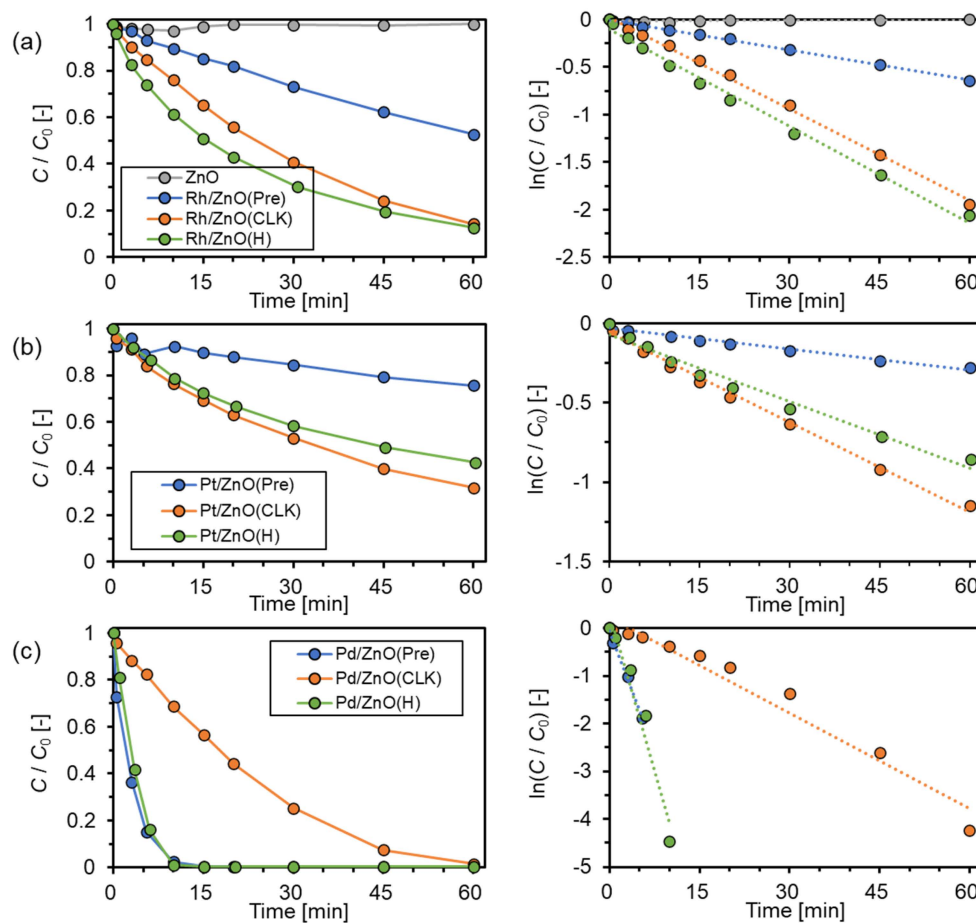


**Figure 8.** Normalized concentration changes of 4-NP ( $C/C_0$ ) and plots of  $\ln(C/C_0)$  as functions of reaction times for (a) Rh/ZnO, (b) Pt/ZnO, and (c) Pd/ZnO. The result of ZnO is shown in the (a) figure for reference.

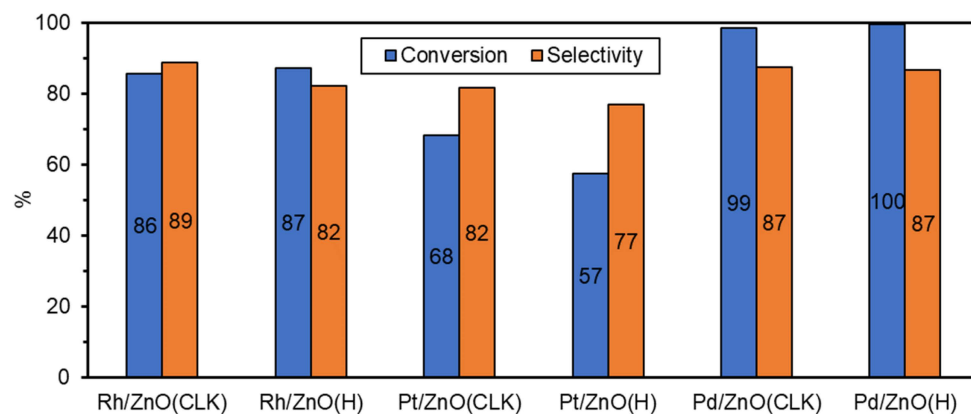


**Figure 9.** Conversions of 4-NP and selectivities to 4-AP after 60 min over the prepared catalysts.

**Table 3.** Summary of amounts of platinum group metals (PGM) in used catalysts and reaction rate constants (k) of this study and previous studies in 4-NP hydrogenation.

Catalyst	PGM Amount [ $\mu\text{g}$ ]	k [ $\text{min}^{-1}$ ]	Reaction Conditions	Ref.
Rh/ZnO(Pre)		0.010		
Rh/ZnO(CLK)		0.032		
Rh/ZnO(H)		0.034		
Pt/ZnO(Pre)		0.004	4-NP (1.6 mM)	
Pt/ZnO(CLK)	500	0.019	NaBH <sub>4</sub> (47 mM)	This study
Pt/ZnO(H)		0.014	10 mg-cat/9 mL	
Pd/ZnO(Pre)		0.328		
Pd/ZnO(CLK)		0.067		
Pd/ZnO(H)		0.439		
Rh NPs stabilized by PVP or CTAC	0.3	0.38–0.70	4-NP (0.1 mM) NaBH <sub>4</sub> (0.005 M)	[56]
Pd NPs stabilized by CTAC		0.03–0.14	0.0032 $\mu\text{mol-cat}/20 \mu\text{L}$	
5.0–8.7 wt%Pd/Fe <sub>3</sub> O <sub>4</sub>	0.4–0.7	0.38–0.75	4-NP (10 mM) NaBH <sub>4</sub> (0.1 M) 0.008 mg-cat/3 mL	[57]
Pd/CNT	n.a.	0.376	4-NP (2 mM) NaBH <sub>4</sub> (0.1 M) 0.3 mg-cat/45 mL	[58]
5 wt%Pd/graphene	200	2.19	4-NP (0.3 mM) NaBH <sub>4</sub> (0.1 M) 4 mg-cat/40 mL	[59]
Pd/graphene oxide	0.02	2.06	4-NP (7.4 mM) NaBH <sub>4</sub> (0.41 M) 7.5 $\mu\text{g-cat}/30 \mu\text{L}$	[60]
Pt NPs stabilized by guar gum	24	0.42	4-NP (1 mM) NaBH <sub>4</sub> (0.1 M) 0.125 mol-cat/50 $\mu\text{L}$	[61]

#### 4. Conclusions

Zinc-rich intermetallic compounds supported on ZnO were prepared using a CaH<sub>2</sub>-assisted molten salt synthesis method. X-ray diffraction measurements suggested the formation of RhZn<sub>13</sub>, Pt<sub>3</sub>Zn<sub>10</sub>, and Pd<sub>5</sub>Zn<sub>8</sub> in the samples reduced by CaH<sub>2</sub> in molten LiCl-KCl, whereas RhZn, PtZn, and PdZn were observed in the samples reduced by hydrogen flow. In the selective hydrogenation of 4-NP to 4-AP, RhZn<sub>13</sub>/ZnO and Pt<sub>3</sub>Zn<sub>10</sub>/ZnO showed almost the same activities as RhZn/ZnO and PtZn/ZnO, respectively, but, interestingly, the zinc-rich catalysts gave higher selectivities. These results indicate that the CaH<sub>2</sub>-assisted molten salt synthesis method has a higher reduction capacity than the common hydrogen-reduction method, which allows for the formation of zinc-rich intermetallic compounds of RhZn<sub>13</sub> and Pt<sub>3</sub>Zn<sub>10</sub>, thus giving rise to an enhancement of the selectivity of the catalytic selective hydrogenation reaction.

**Author Contributions:** Conceptualization, Y.K.; methodology, Y.K. and K.Y.; validation, Y.K.; formal analysis, Y.K.; investigation, Y.K. and R.S.; resources, Y.K. and R.S.; data curation, Y.K. and K.Y.; writing—original draft preparation, Y.K.; writing—review and editing, Y.K., K.Y. and R.S.; visualization, Y.K.; supervision, Y.K.; project administration, Y.K.; funding acquisition, Y.K. and R.S. All authors have read and agreed to the published version of the manuscript.

**Funding:** This research was funded by the Japan Society for the Promotion of Science (JSPS), grant number 21K14465.

**Data Availability Statement:** Data are contained within the article.

**Acknowledgments:** The authors thank Masanao Narita at the Renewable Energy Research Centre, National Institute of Advanced Industrial Science and Technology for SEM observations.

**Conflicts of Interest:** The authors declare no conflicts of interest.

## References

1. Bartholomew, C.H.; Farrauto, R.J. Hydrogenation and Dehydrogenation of Organic Compounds. In *Fundamentals of Industrial Catalytic Processes*, 2nd ed.; John Wiley & Sons, Inc.: Hoboken, NJ, USA, 2006; pp. 487–559.
2. Soma-Noto, Y.; Sachtler, W.M.H. Infrared spectra of carbon monoxide adsorbed on supported palladium and palladium-silver alloys. *J. Catal.* **1974**, *32*, 315–324. [[CrossRef](#)]
3. Boudart, M. Catalysis by Supported Metals. *Adv. Catal.* **1969**, *20*, 153–166. [[CrossRef](#)]
4. Vargheese, V.; Ghampson, I.T.; Yun, G.-N.; Kobayashi, Y.; Takagaki, A.; Oyama, S.T. A New One-Pot Sequential Reduction-Deposition Method for the synthesis of Silica-supported NiPt and CuPt Bimetallic Catalysts. *Appl. Catal. A* **2020**, *591*, 117371. [[CrossRef](#)]
5. Liao, F.; Lo, T.W.B.; Tsang, S.C.E. Recent Developments in Palladium-Based Bimetallic Catalysts. *ChemCatChem* **2015**, *7*, 1998–2014. [[CrossRef](#)]
6. Tsai, A.P.; Kameoka, S.; Nozawa, K.; Shimoda, M.; Ishii, Y. Intermetallic: A Pseudoelement for Catalysis. *Acc. Chem. Res.* **2017**, *50*, 2879–2885. [[CrossRef](#)] [[PubMed](#)]
7. Fang, H.; Yang, J.; Wen, M.; Wu, Q. Nanoalloy Materials for Chemical Catalysis. *Adv. Mater.* **2018**, *30*, 1705698. [[CrossRef](#)] [[PubMed](#)]
8. Zhu, L.; Li, C.; Yun, Q.; Han, S.; Lv, Y.; Lu, Q.; Chen, J. Recent advances of Rh-based intermetallic nanomaterials for catalytic applications. *Chin. Chem. Lett.* **2023**, *34*, 108515. [[CrossRef](#)]
9. Xia, Y.; Wang, Z.; Feng, Y.; Xie, S.; Liu, Y.; Dai, H.; Deng, J. In situ molten salt derived iron oxide supported platinum catalyst with high catalytic performance for o-xylene elimination. *Catal. Today* **2020**, *351*, 30–36. [[CrossRef](#)]
10. Carvalho, M.S.; Lacerda, R.A.; Leão, J.P.B.; Scholten, J.D.; Neto, B.A.D.; Suarez, P.A.Z. In situ generated palladium nanoparticles in imidazolium-based ionic liquids: A versatile medium for an efficient and selective partial biodiesel hydrogenation. *Catal. Sci. Technol.* **2011**, *1*, 480–488. [[CrossRef](#)]
11. Lacarbonara, G.; Chini, S.; Ratso, S.; Kruusenberg, I.; Arbizzani, C. A MnO<sub>x</sub>-graphitic carbon composite from CO<sub>2</sub> for sustainable Li-ion battery anodes. *Mater. Adv.* **2022**, *3*, 7087–7097. [[CrossRef](#)]
12. Najafli, E.; Ratso, S.; Ivanov, Y.P.; Gatalo, M.; Pavko, L.; Yörük, C.R.; Walke, P.; Divitini, G.; Hodnik, N.; Kruusenberg, I. Sustainable CO<sub>2</sub>-Derived Nanoscale Carbon Support to a Platinum Catalyst for Oxygen Reduction Reaction. *ACS Appl. Nano Mater.* **2023**, *6*, 5772–5780. [[CrossRef](#)]
13. Kobayashi, Y. Synthesis of Porous Ni<sub>3</sub>Al Intermetallic Nano-compounds in a Molten LiCl with Assistance of CaH<sub>2</sub> as a Structure-controlling Agent. *Chem. Lett.* **2019**, *48*, 1496–1499. [[CrossRef](#)]
14. Kobayashi, Y.; Tada, S.; Mizoguchi, H. Chemical route to prepare nickel supported on intermetallic Ti<sub>6</sub>Si<sub>7</sub>Ni<sub>16</sub> nanoparticles catalyzing CO methanation. *Nanoscale* **2021**, *13*, 16533–16542. [[CrossRef](#)] [[PubMed](#)]
15. Kobayashi, Y.; Yokoyama, S.; Shoji, R. Molten salt synthesis of intermetallic compound TiNi nanopowder passivated by TiO<sub>x</sub> shell prepared from NiTiO<sub>3</sub> for catalytic hydrogenation. *Materials* **2022**, *15*, 8536. [[CrossRef](#)] [[PubMed](#)]
16. Kobayashi, Y.; Tada, S.; Kondo, M.; Fujiwara, K.; Mizoguchi, H. Intermetallic YIr<sub>2</sub> nanoparticles with negatively charged Ir active sites for catalytic hydrogenation of cyclohexanone to cyclohexanol. *Catal. Sci. Technol.* **2022**, *12*, 3088–3093. [[CrossRef](#)]
17. Kobayashi, Y.; Tada, S.; Kondo, M.; Fujiwara, K.; Mizoguchi, H. Superior catalytic performance of intermetallic CaPt<sub>2</sub> nanoparticles supported on titanium group oxides in hydrogenation of ketones to alcohols. *Chem. Commun.* **2022**, *58*, 4795–4798. [[CrossRef](#)]
18. Kobayashi, Y.; Sohmiya, M.; Tada, S.; Kikuchi, R. Low-temperature Synthesis of Single Phase Intermetallic NiZn Bulk Nanopowder in Molten LiCl–KCl with CaH<sub>2</sub> Reducing Agent. *J. Japan Pet. Inst.* **2020**, *63*, 380–387. [[CrossRef](#)]
19. Furukawa, S.; Takahashi, K.; Komatsu, T. Well-structured bimetallic surface capable of molecular recognition for chemoselective nitroarene hydrogenation. *Chem. Sci.* **2016**, *7*, 4476–4484. [[CrossRef](#)]
20. Miyazaki, M.; Furukawa, S.; Komatsu, T. Regio- and chemoselective hydrogenation of dienes to monoenes governed by a well-structured bimetallic surface. *J. Am. Chem. Soc.* **2017**, *139*, 18231–18239. [[CrossRef](#)]
21. Silvestre-Albero, J.; Serrano-Ruiz, J.C.; Sepúlveda-Escribano, A.; Rodríguez-Reinoso, F. Modification of the catalytic behavior of platinum by zinc in crotonaldehyde hydrogenation and iso-butane dehydrogenation. *Appl. Catal. A Gen.* **2005**, *292*, 244–251. [[CrossRef](#)]
22. Silvestre-Albero, J.; Coloma, F.; Sepúlveda-Escribano, A.; Rodríguez-Reinoso, F. Effect of the presence of chlorine in bimetallic PtZn/CeO<sub>2</sub> catalysts for the vapor-phase hydrogenation of crotonaldehyde. *Appl. Catal. A Gen.* **2006**, *304*, 159–167. [[CrossRef](#)]
23. Galloway, E.; Armbrüster, M.; Kovnir, K.; Tikhov, M.S.; Lambert, R.M. Bromine-promoted PtZn is very effective for the chemoselective hydrogenation of crotonaldehyde. *J. Catal.* **2009**, *261*, 60–65. [[CrossRef](#)]
24. Han, A.; Zhang, J.; Sun, W.; Chen, W.; Zhang, S.; Han, Y.; Feng, Q.; Zheng, L.; Gu, L.; Chen, C.; et al. Isolating contiguous Pt atoms and forming Pt–Zn intermetallic nanoparticles to regulate selectivity in 4-nitrophenylacetylene hydrogenation. *Nat. Comm.* **2019**, *10*, 3787. [[CrossRef](#)]

25. Jin, Y.; Ren, G.; Feng, Y.; Geng, S.; Li, L.; Zhu, X.; Guo, J.; Shao, Q.; Xu, Y.; Huang, X.; et al. A top-down strategy to realize the synthesis of small-sized L10-platinum-based intermetallic compounds for selective hydrogenation. *Nano Res.* **2022**, *15*, 9631–9638. [[CrossRef](#)]
26. Iihama, S.; Furukawa, S.; Komatsu, T. Efficient catalytic system for chemoselective hydrogenation of halonitrobenzene to haloaniline using PtZn intermetallic compound. *ACS Catal.* **2016**, *6*, 742–746. [[CrossRef](#)]
27. Smirnova, N.S.; Khramov, E.V.; Stolarov, I.P.; Yakushev, I.A.; Baeva, G.N.; Bragina, G.O.; Belova, E.V.; Ishchenko, A.V.; Popova, A.S.; Zubavichus, Y.V.; et al. Nanostructured PtZn intermetallic compound: Controlled formation from PtZn(CH<sub>3</sub>COO)<sub>4</sub> molecular precursor and tests of catalytic properties. *Intermetallics* **2021**, *132*, 107160. [[CrossRef](#)]
28. Tew, M.W.; Emerich, H.; van Bokhoven, J.A. Formation and Characterization of PdZn Alloy: A Very Selective Catalyst for Alkyne Semihydrogenation. *J. Phys. Chem. C* **2011**, *115*, 8457–8465. [[CrossRef](#)]
29. Mashkovsky, I.S.; Markov, P.V.; Bragina, G.O.; Rassolov, A.V.; Baeva, G.N.; Stakheev, A.Y. Intermetallic Pd<sub>1</sub>–Zn<sub>1</sub> nanoparticles in the selective liquid-phase hydrogenation of substituted alkynes. *Kinet. Catal.* **2017**, *58*, 480–491. [[CrossRef](#)]
30. Mashkovsky, I.S.; Markov, P.V.; Bragina, G.O.; Baeva, G.N.; Rassolov, A.V.; Bukhtiyarov, A.V.; Prosvirin, I.P.; Bukhtiyarov, V.I.; Stakheev, A.Y. PdZn/ $\alpha$ -Al<sub>2</sub>O<sub>3</sub> catalyst for liquid-phase alkyne hydrogenation: Effect of the solid-state alloy transformation into intermetallics. *Mendeleev Commun.* **2018**, *28*, 152–154. [[CrossRef](#)]
31. Zhou, H.; Yang, X.; Wang, A.; Miao, S.; Liu, X.; Pan, X.; Su, Y.; Li, L.; Tan, Y.; Zhang, T. Pd/ZnO catalysts with different origins for high chemoselectivity in acetylene semi-hydrogenation. *Chin. J. Catal.* **2016**, *37*, 692–699. [[CrossRef](#)]
32. Zhou, H.; Yang, X.; Li, L.; Liu, X.; Huang, Y.; Pan, X.; Wang, A.; Li, J.; Zhang, T. PdZn intermetallic nanostructure with Pd–Zn–Pd ensembles for highly active and chemoselective semi-hydrogenation of acetylene. *ACS Catal.* **2016**, *6*, 1054–1061. [[CrossRef](#)]
33. Glyzdova, D.V.; Smirnova, N.S.; Leont'eva, N.N.; Gerasimov, E.Y.; Prosvirin, I.P.; Vershinin, V.I.; Shlyapina, D.A.; Tsyru'nikov, P.G. Synthesis and characterization of Sibunit-supported Pd–Ga, Pd–Zn, and Pd–Ag catalysts for liquid-phase acetylene hydrogenation. *Kinet. Catal.* **2017**, *58*, 140–146. [[CrossRef](#)]
34. Glyzdova, D.V.; Smirnova, N.S.; Temerev, V.L.; Khramov, E.V.; Gulyaeva, T.I.; Trenikhin, M.V.; Shlyapin, D.A.; Tsyru'nikov, P.G. Study of the Influence Exerted by Zinc Additive on the Structure and Catalytic Properties of Pd/Al<sub>2</sub>O<sub>3</sub> Catalysts for Liquid-Phase Hydrogenation of Acetylene. *Russ. J. Appl. Chem.* **2017**, *90*, 1908–1917. [[CrossRef](#)]
35. Meunier, F.; Maffre, M.; Schuurman, Y.; Colussi, S.; Trovarelli, A. Acetylene semi-hydrogenation over Pd–Zn/CeO<sub>2</sub>: Relevance of CO adsorption and methanation as descriptors of selectivity. *Catal. Comm.* **2018**, *105*, 52–55. [[CrossRef](#)]
36. Hu, M.; Zhao, S.; Liu, S.; Chen, C.; Chen, W.; Zhu, W.; Liang, C.; Cheong, W.C.; Wang, Y.; Yu, Y.; et al. MOF-Confined Sub-2 nm Atomically Ordered Intermetallic PdZn Nanoparticles as High-Performance Catalysts for Selective Hydrogenation of Acetylene. *Adv. Mater.* **2018**, *30*, 1801878. [[CrossRef](#)] [[PubMed](#)]
37. Glyzdova, D.V.; Vedyagin, A.A.; Tsapina, A.M.; Kaichev, V.V.; Trigub, A.L.; Trenikhin, M.V.; Shlyapin, D.A.; Tsyru'nikov, P.G.; Lavrenov, A.V. A study on structural features of bimetallic Pd–M/C (M: Zn, Ga, Ag) catalysts for liquid-phase selective hydrogenation of acetylene. *Appl. Catal. A Gen.* **2018**, *563*, 18–27. [[CrossRef](#)]
38. Yang, L.; Guo, Y.; Long, J.; Xia, L.; Li, D.; Xiao, J.; Liu, H. PdZn alloy nanoparticles encapsulated within a few layers of graphene for efficient semi-hydrogenation of acetylene. *Chem. Commun.* **2019**, *55*, 14693–14696. [[CrossRef](#)]
39. Glyzdova, D.V.; Afonassenko, T.N.; Khramov, E.V.; Leont'eva, N.N.; Trenikhin, M.V.; Prosvirin, I.P.; Bukhtiyarov, A.V.; Shlyapin, D.A. Zinc Addition Influence on the Properties of Pd/Sibunit Catalyst in Selective Acetylene Hydrogenation. *Top. Catal.* **2020**, *63*, 139–151. [[CrossRef](#)]
40. Glyzdova, D.V.; Afonassenko, T.N.; Temerev, V.L.; Shlyapin, D.A. Acetylene Hydrogenation on Pd–Zn/Sibunit Catalyst: Effect of Solvent and Carbon Monoxide. *Pet. Chem.* **2021**, *61*, 490–497. [[CrossRef](#)]
41. Cao, X.; Tong, R.; Tang, S.; Jang, B.W.-L.; Mirjalili, A.; Li, J.; Guo, X.; Zhang, J.; Hu, J.; Meng, X. Design of Pd–Zn Bimetal MOF Nanosheets and MOF-Derived Pd<sub>3.9</sub>Zn<sub>6.1</sub>/CNS Catalyst for Selective Hydrogenation of Acetylene under Simulated Front-End Conditions. *Molecules* **2022**, *27*, 5736. [[CrossRef](#)]
42. Glyzdova, D.V.; Afonassenko, T.N.; Khramov, E.V.; Trenikhin, M.V.; Prosvirin, I.P.; Shlyapin, D.A. Effect of Reductive Treatment Duration on the Structure and Properties of Pd–Zn/C Catalysts for Liquid-Phase Acetylene Hydrogenation. *ChemCatChem* **2022**, *14*, e202200893. [[CrossRef](#)]
43. Tiwari, G.; Sharma, G.; Verma, R.; Gakhad, P.; Singh, A.K.; Polshettiwar, V.; Jagirdar, B.R. Acetylene Semi-Hydrogenation at Room Temperature over Pd–Zn Nanocatalyst. *Chem. Eur. J.* **2023**, *29*, e202301932. [[CrossRef](#)]
44. Shen, L.; Mao, S.; Li, J.; Li, M.; Chen, P.; Li, H.; Chen, Z.; Wang, Y. PdZn intermetallic on a CN@ZnO hybrid as an efficient catalyst for the semihydrogenation of alkynols. *J. Catal.* **2017**, *350*, 13–20. [[CrossRef](#)]
45. Chen, X.; Shi, C.; Wang, X.-B.; Li, W.-Y.; Liang, C. Intermetallic PdZn nanoparticles catalyze the continuous-flow hydrogenation of alkynols to cis-enols. *Comm. Chem.* **2021**, *4*, 175. [[CrossRef](#)]
46. Zhu, H.; Zhao, H.; Ma, H.; Li, B.; Kou, J.; Li, J.; Gao, M.; Zeng, G.; Fang, J.; Dong, Z. Ultrafine PdZn bimetallic nanoparticles anchored on sulfur-doped mesoporous carbon for the partial hydrogenation of alkynols. *Catal. Today* **2022**, *405–406*, 242–250. [[CrossRef](#)]
47. Ye, C.; Chen, X.; Li, S.; Feng, B.; Fu, Y.; Zhang, F.; Chen, D.-L.; Zhu, W. PdZn intermetallic compound stabilized on ZnO/nitrogen-decorated carbon hollow spheres for catalytic semihydrogenation of alkynols. *Nano Res.* **2022**, *15*, 3090–3098. [[CrossRef](#)]
48. Sarkany, A.; Zsoldos, Z.; Furlong, B.; Hightower, J.W.; Gucci, L. Hydrogenation of 1-Butene and 1,3-Butadiene Mixtures over Pd/ZnO Catalysts. *J. Catal.* **1993**, *141*, 566–582. [[CrossRef](#)]

49. Castillejos-López, E.; Agostini, G.; Michel, M.D.; Iglesias-Juez, A.; Bachiller-Baeza, B. Synergy of contact between ZnO surface planes and PdZn nanostructures: Morphology and chemical property effects in the intermetallic sites for selective 1,3-butadiene hydrogenation. *ACS Catal.* **2017**, *7*, 796–811. [[CrossRef](#)]
50. Vernuccio, S.; Goy, R.; von Rohr, P.R.; Medlock, J.; Bonrath, W. Hydrogenation of 2-methyl-3-butyn-2-ol over a Pd/ZnO catalyst: Kinetic model and selectivity study. *React. Chem. Eng.* **2016**, *1*, 445–453. [[CrossRef](#)]
51. Okhlopkova, L.B.; Kerzhentseva, M.A.; Ismagilov, Z.R. Internal Surface Coating of a Capillary Microreactor for the Selective Hydrogenation of 2-Methyl-3-Butyn-2-Ol Using a PdZn/TiO<sub>2</sub> Catalyst. The Effect of the Catalyst's Activation Conditions on Its Catalytic Properties. *Kinet. Catal.* **2018**, *59*, 347–356. [[CrossRef](#)]
52. Okhlopkova, L.B.; Cherepanova, S.V.; Prosvirin, I.P.; Kerzhentsev, M.A.; Ismagilov, Z.R. Semihydrogenation of 2-methyl-3-butyn-2-ol on Pd-Zn nanoalloys: Effect of composition and heterogenization. *Appl. Catal. A Gen.* **2018**, *549*, 245–253. [[CrossRef](#)]
53. Furukawa, S.; Yoshida, Y.; Komatsu, T. Chemoselective hydrogenation of nitrostyrene to aminostyrene over Pd- and Rh-based intermetallic compounds. *ACS Catal.* **2014**, *4*, 1441–1450. [[CrossRef](#)]
54. Fujita, S.; Mitani, H.; Zhang, C.; Li, K.; Zhao, F.; Arai, M. Pd and PdZn supported on ZnO as catalysts for the hydrogenation of cinnamaldehyde to hydrocinnamyl alcohol. *Mol. Catal.* **2017**, *442*, 12–19. [[CrossRef](#)]
55. Zhang, L.; Zhong, Y.; Wang, J.; Zeng, Z.; Deng, S.; Zou, J.-J.; Deng, Q. Intermetallic Palladium–Zinc Nanoparticles for the Ultrasensitive Hydrogenative Rearrangement of Furan Compounds. *ACS Catal.* **2023**, *13*, 13205–13214. [[CrossRef](#)]
56. Yanilkin, V.V.; Nastapova, N.V.; Nasretdinova, G.R.; Osin, Y.N.; Evtjugin, V.G.; Ziganshina, A.Y.; Gubaidullin, A.T. Structure and catalytic activity of ultrasmall Rh, Pd and (Rh + Pd) nanoparticles obtained by mediated electrosynthesis. *New J. Chem.* **2019**, *43*, 3931–3945. [[CrossRef](#)]
57. Gregor, L.; Reilly, A.K.; Dickstein, T.A.; Mazhar, S.; Bram, S.; Morgan, D.G.; Losovyj, Y.; Pink, M.; Stein, B.D.; Matveeva, V.G.; et al. Facile synthesis of magnetically recoverable Pd and Ru catalysts for 4-nitrophenol reduction: Identifying key factors. *ACS Omega* **2018**, *3*, 14717–14725. [[CrossRef](#)]
58. Kim, J.D.; Choi, M.Y.; Choi, H.C. Catalyst activity of carbon nanotube supported Pd catalysts for the hydrogenation of nitroarenes. *Mater. Chem. Phys.* **2016**, *173*, 404–411. [[CrossRef](#)]
59. Sun, J.; Fu, Y.; He, G.; Sun, X.; Wang, X. Catalytic hydrogenation of nitrophenols and nitrotoluenes over a palladium/graphene nanocomposite. *Catal. Sci. Technol.* **2014**, *4*, 1742–1748. [[CrossRef](#)]
60. Sun, W.; Lu, X.; Tong, Y.; Zhang, Z.; Lei, J.; Nie, G.; Wang, C. Fabrication of highly dispersed palladium/graphene oxide nanocomposites and their catalytic properties for efficient hydrogenation of *p*-nitrophenol and hydrogen generation. *Int. J. Hydrogen Energy* **2014**, *39*, 9080–9086. [[CrossRef](#)]
61. Pandey, S.; Mishra, S.B. Catalytic reduction of *p*-nitrophenol by using platinum nanoparticles stabilised by guar gum. *Carbohydr. Polym.* **2014**, *113*, 525–531. [[CrossRef](#)]

**Disclaimer/Publisher's Note:** The statements, opinions and data contained in all publications are solely those of the individual author(s) and contributor(s) and not of MDPI and/or the editor(s). MDPI and/or the editor(s) disclaim responsibility for any injury to people or property resulting from any ideas, methods, instructions or products referred to in the content.